

Vision Backbone Enhancement via Multi-Stage Cross-Scale Attention

Liang Shang¹, Yanli Liu², Zhengyang Lou¹, Shuxue Quan², Nagesh Adluru¹,
Bochen Guan², and William A. Sethares¹

August 16, 2023

Abstract

Convolutional neural networks (CNNs) and vision transformers (ViTs) have achieved remarkable success in various vision tasks. However, many architectures do not consider interactions between feature maps from different stages and scales, which may limit their performance. In this work, we propose a simple add-on attention module to overcome these limitations via multi-stage and cross-scale interactions. Specifically, the proposed Multi-Stage Cross-Scale Attention (MSCSA) module takes feature maps from different stages to enable multi-stage interactions and achieves cross-scale interactions by computing self-attention at different scales based on the multi-stage feature maps. Our experiments on several downstream tasks show that MSCSA provides a significant performance boost with modest additional FLOPs and runtime.

1 Introduction

Convolutional neural networks (CNNs) and vision transformers (ViTs) have been widely used as backbones in various vision tasks, such as image classification [34, 17], object detection [23, 24, 44], semantic segmentation [5, 54, 69], video recognition [53, 18], and medical imaging [43, 52]. However, many existing architectures do not fully exploit interactions between feature maps from different stages and different scales, which may restrict their performance on downstream tasks.

For example, in object detection, the connections between smaller and larger parts of an object and objects of different sizes are essential for accurate localization. Similarly, in semantic segmentation, the correlations between representative and abstract feature maps at different stages of a network can be critical for accurate predictions. However, these interactions may be missed in traditional single-path top-to-bottom architectures.

The first type of connection can be incorporated by allowing interactions between image patches of different scales. We call this *cross-scale interaction*. For CNNs, shortcut connections [24, 28] and other architectural topologies [57, 58, 56, 19, 62], namely different ways of connecting feature aggregation modules, can be used to explore the interaction between feature maps in different scales. Similarly, ViTs also try to address this issue in various ways. For instance, [70, 76, 21, 3, 36, 37] extend the idea of cross-scale interactions to several network topologies for fusing feature maps. Others [78, 66, 8, 67, 72, 71] propose modifying existing modules to introduce cross-scale interactions.

The correlations between representative and abstract feature maps can be modeled by allowing the feature maps to interact between different stages of the backbone. We call this *multi-stage interaction*. To incorporate multi-stage interaction, CoaT [70] and TopFormer [81] propose parallel branches to connect feature maps at different stages. However, these approaches have limitations. CoaT’s Co-Scale mechanism is computationally complex and is limited to a specific backbone structure, while TopFormer only downsamples feature maps in the parallel branch, which limits interactions to multiple stages but not across scales.

In this work, we propose a simple add-on attention module, *Multi-Stage Cross-Scale Attention (MSCSA)*, to enhance both multi-stage and cross-scale interactions in CNN and ViT backbones, as

¹University of Wisconsin - Madison, Madison, WI, US. lshang6@wisc.edu, zlou4@wisc.edu, adluru@wisc.edu, sethares@wisc.edu

²OPPO US Research Center, Palo Alto, CA, US. yanli.liu@oppo.com, quanshuxue@gmail.com, bochen.guan@oppo.com

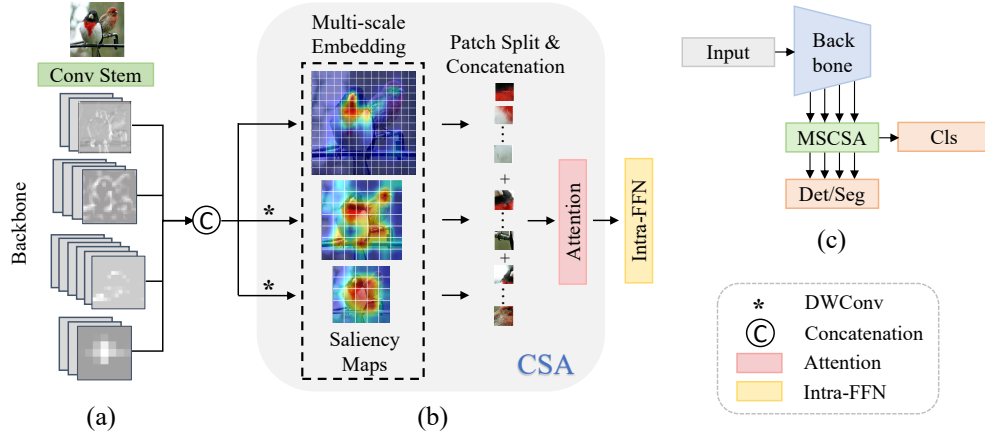


Figure 1: (a) **Feature aggregation for multi-stage interaction.** In MSCSA, the output feature maps from different stages of the backbone are downsampled and concatenated along the channel dimension to enable multi-stage interaction. (b) **Cross-scale attention (CSA) and Intra-FFN.** CSA first applies depthwise convolutions to generate key and value tensors at different scales, then concatenates them to compute an attention map across scales. Intra-FFN only carries out FFN computation within each stage to save FLOPs. (c) **MSCSA as an add-on module for vision backbones.** MSCSA is designed as an add-on module that takes feature maps from different stages of the vision backbone as input. The output of MSCSA can be used for various downstream tasks such as classification, detection, and segmentation.

illustrated in Fig. 1. Our approach combines Cross-Scale Attention (CSA) and Intra-Feed-Forward Networks (Intra-FFN) to achieve these interactions with moderate additional computational cost.

Specifically, to enable multi-stage interactions, we collect feature maps from different stages of the backbone and concatenate them as a multi-stage feature map, as shown in Fig. 1a. To achieve cross-scale interactions, we first apply depthwise convolutions in CSA to obtain embeddings at different scales, where an example of the saliency maps of these multi-scale feature embeddings are depicted in Fig. 1b. These saliency maps illustrate that the features in coarser scales focus more on the overall objects of interest, while the features in finer scales focus on different parts of the birds, *e.g.*, the beak in the top scale and the feet in the middle scale. These multi-scale embeddings are then concatenated and used to compute a cross-scale attention map to exploit information across multiple scales. Furthermore, we replace half of the usual feed-forward networks (FFNs) with the Intra-FFN, which only carries out intra-stage FFN computation and saves FLOPs in compensation for the additional computation in CSA.

We conduct experiments on several CNN and ViT-based vision backbones, including TopFormer [81], CoaT [70], ResNet [24], PVTv2 [65], Swin [44], and the state-of-the-art models P2T [67] and ConvNeXt [45] on common benchmark tasks to validate the effectiveness of MSCSA. Our results show that MSCSA provides a significant performance boost on these backbones, especially on downstream tasks. Furthermore, this improvement only comes with modest increases in FLOPs and runtime.

Our contributions can be summarized as follows:

1. We propose Cross-Scale Attention (CSA) and Intra-Feed-Forward Networks (Intra-FFN) to enable multi-stage and cross-scale feature interactions in an efficient manner.
2. We design Multi-Stage Cross-Scale Attention (MSCSA) as an add-on module that applies to a variety of vision backbones and leads to a clear performance boost.
3. We demonstrate that MSCSA brings a clear performance boost on various vision backbones. In most cases, this comes with less than 10% additional FLOPs and runtime.

2 Related Works

Vision Transformers (ViTs). The introduction of vision transformers (ViTs) in [17] generated significant interest, and standard training strategies are provided by DeiT [59]. However, the quadratic complexity of the self-attention mechanism [61] leads to a heavy computational burden for ViTs. To

overcome this, Swin Transformer [44] proposes computing the self-attention within local windows, a strategy that has been widely applied and developed in subsequent works [16, 50, 30, 6, 21, 22, 68, 73]. Other recent papers [74, 40, 66, 60] aim to improve the performance further by managing the global interactions between windows. Additionally, some works [64, 65, 18, 38, 80, 73, 67, 9, 48, 72] use feature down-sampling within the attention blocks to reduce the computational cost.

Multi-stage and cross-scale interaction in ViTs. As the ViT research community grows, researchers have started exploring new ViT topology designs. CoaT [70] and TopFormer [81] build parallel paths to add connections between feature maps in different stages, while CoaT further employs cross-scale interactions by keeping feature maps in different resolutions in the parallel path. CrossViT [3] proposes a dual-path architecture of different patch sizes, where the cross-scale interactions occur through the classification (CLS) tokens [15, 17, 59] when exchanging between the paths. Inspired by HRNet [62], HRFormer [76] and HRViT [21] maintain several feature paths of different resolutions to apply cross-scale interactions. LG-Transformer [37] and MPViT [36] generate multiple paths of varying resolutions in the single-stage block structure and add cross-scale interactions within the stage.

In contrast, many other works focus on modifying specific modules within the ViT architecture to achieve cross-scale interactions. CrossFormer [66], DPT [8], and PatchFormer [78] generate multi-scale feature maps in patch embedding layers, while Focal [72], LVT [71], Shunted [51], and P2T [67] suggest using multi-scale feature embeddings for key and value tensors or query tensors in the attention blocks.

Comparison to previous works. MSCSA applies a tailored attention mechanism in a parallel branch to achieve effective multi-stage and cross-scale interactions. In contrast, CoaT [70] only uses simple operations such as addition and pooling/upsampling to fuse feature maps from different scales, while other models mainly focus on one of the multi-stage and cross-scale interactions.

Moreover, MSCSA applies to popular CNN and ViT backbones. In comparison, many existing cross-scale and multi-stage interactions are designed for certain backbones. For instance, HRViT [21] and HRFormer [76] inherit the HRNet [62] structure, which makes them not directly applicable to other backbones. The Pooling-based MHSA in P2T [67] and the Shunted Self-Attention [51] maintains multi-scale embedding in their attention block, which makes them not directly applicable to window-based attentions with global interactions [74, 40, 66, 60]. To the best of our knowledge, MSCSA is the first add-on module that boosts the performance of vision backbones with efficient multi-stage cross-scale interactions.

3 Multi-Stage Cross-Scale Attention Design

3.1 Overview

Multi-Stage Cross-Scale Attention (Fig. 4) is a lightweight add-on module capable of incorporating multi-stage and cross-scale interactions. It is designed to boost the performance of popular vision backbones with only a modest increase in computation (approximately 10% more FLOPs). To achieve efficient multi-stage interactions, MSCSA first collects feature maps from different stages of a vision backbone, downsamples, and combines them along the channel dimension to obtain a multi-stage feature map. Then, cross-scale interactions are performed by Cross-Scale Attention (CSA), as in Fig. 2, where the key and value tensors contain information from feature maps of different scales. To allow for the additional computational cost in MSCSA, we replace half of the Feed-Forward Networks (FFNs) after the CSA with an Intra-Feed-Forward Network (Intra-FFN), where the comparison between FFN and Intra-FFN is illustrated in Fig. 3.

This section introduces the CSA mechanism and Intra-FFN in Secs. 3.2 and 3.3, respectively. Several architectural variants of MSCSA designed for different tasks are discussed in Sec. 3.4. The examples of applying MSCSA to various vision backbones can be found in the Appendix.

3.2 Cross-Scale Attention (CSA)

CSA aims to perform interactions across coarse and fine scales, it introduces interactions between feature maps of different scales, which is desirable for downstream tasks. In contrast to commonly used multi-head self-attention [61, 17, 59] mechanisms, our CSA uses Multi-Scale key, value tensor Projections (MSP), and a Parallel Convolution Path (PCP) [21], as illustrated in Fig. 2.

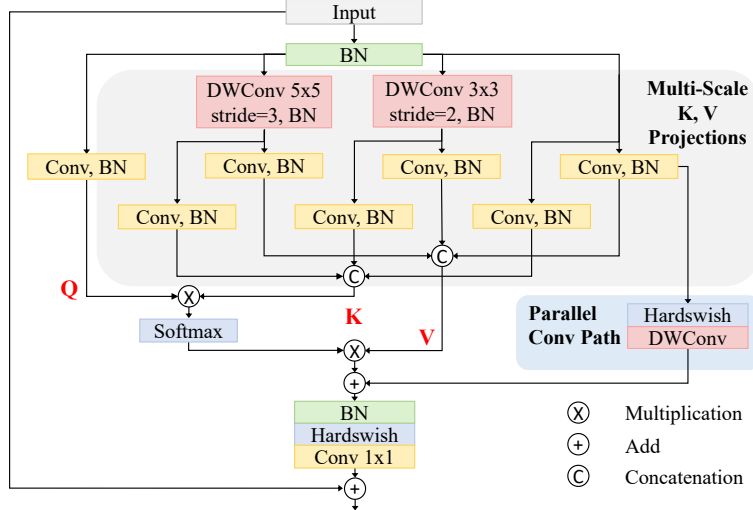


Figure 2: **Cross-Scale Attention**. The CSA consists of Q projection, Multi-Scale K, V Projections (MSP), and a Parallel Convolution Path (PCP) [21]. The multi-scale K, V projections generate the key, value tensors in three different scales, while the parallel convolution path acts as the relative position encoding.

Multi-Scale key, value tensor Projections. A natural way to incorporate cross-scale interactions in self-attention is to use multi-scale feature maps in the attention mechanism. Here, we introduce the multi-scale projections for key and value tensors, where the combined key and value tensors consist of feature maps from the original scale and two downsampled scales. When computing the attention map, every token, *i.e.*, image patch, in the query tensor can query information in the key tensor from three different scales. The output of the self-attention is then a weighted sum of features from different scales.

Specifically, from the input feature map $\mathbf{X} \in \mathbb{R}^{h \times w \times c}$ where h, w, c are the height, width, and channel dimension, respectively, the query tensor \mathbf{Q} can be computed from a linear projection

$$\mathbf{Q} = \mathbf{X}\mathbf{W}^q \in \mathbb{R}^{h \times w \times d} \quad (1)$$

following the original attention mechanism [61] with d being the head dimension. On the other hand, for the key tensor \mathbf{K} and value tensor \mathbf{V} , the input \mathbf{X} is first downsampled using two depthwise convolutional operators:

$$\begin{aligned} \mathbf{X}_0 &= \mathbf{X}, \\ \mathbf{X}_1 &= \text{DWConv}_1(\mathbf{X}), \\ \mathbf{X}_2 &= \text{DWConv}_2(\mathbf{X}), \end{aligned} \quad (2)$$

where \mathbf{X}_i has a size of $h_i \times w_i \times c$ for $i = 0, 1, 2$ as

$$\begin{aligned} h_0 &= h, & w_0 &= w, \\ h_1 &= \left\lfloor \frac{h-1}{2} + 1 \right\rfloor, & w_1 &= \left\lfloor \frac{w-1}{2} + 1 \right\rfloor, \\ h_2 &= \left\lfloor \frac{h-1}{3} + 1 \right\rfloor, & w_2 &= \left\lfloor \frac{w-1}{3} + 1 \right\rfloor, \end{aligned} \quad (3)$$

and DWConv_1 is a depthwise convolution for $2 \times$ downsampling, while DWConv_2 achieves $3 \times$ downsampling. Afterwards, the feature maps in different scales $\mathbf{X}_0, \mathbf{X}_1, \mathbf{X}_2$ generate their key and value tensors via linear projections separately:

$$\begin{aligned} \mathbf{K}_0 &= \mathbf{X}_0 \mathbf{W}_0^k, & \mathbf{V}_0 &= \mathbf{X}_0 \mathbf{W}_0^v, \\ \mathbf{K}_1 &= \mathbf{X}_1 \mathbf{W}_1^k, & \mathbf{V}_1 &= \mathbf{X}_1 \mathbf{W}_1^v, \\ \mathbf{K}_2 &= \mathbf{X}_2 \mathbf{W}_2^k, & \mathbf{V}_2 &= \mathbf{X}_2 \mathbf{W}_2^v, \end{aligned} \quad (4)$$

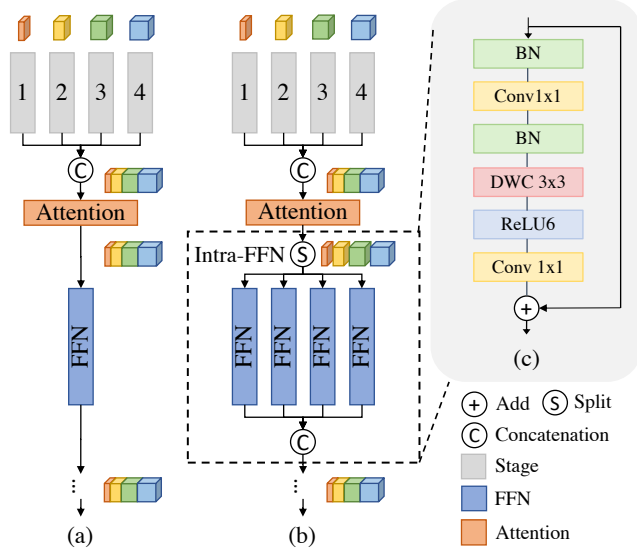


Figure 3: **FFN and Intra-FFN.** (a) The commonly used self-attention and FFN. (b) The self-attention followed by our proposed Intra-FFN. (c) The detailed architecture of FFN. In Intra-FFN, the feature map is first split into four parts corresponding to the channel dimension in each stage and then fed into four FFNs separately.

where \mathbf{K}_i has a size of $h_i w_i \times d$ and \mathbf{V}_i has a size of $h_i w_i \times 2d$ for $i = 0, 1, 2$. Following the dimension settings of LeViT [20], the value tensors have twice the head dimension as the query and key tensors have. As $2d$ could be the commonly used head dimension in self-attention in other works, the computational cost of our attention is reduced. These key and value tensors representing different scales are then concatenated together to form the multi-scale key and value tensors

$$\begin{aligned}\mathbf{K} &= \text{Concat}(\mathbf{K}_0, \mathbf{K}_1, \mathbf{K}_2), \\ \mathbf{V} &= \text{Concat}(\mathbf{V}_0, \mathbf{V}_1, \mathbf{V}_2),\end{aligned}\quad (5)$$

where the concatenated \mathbf{K} and \mathbf{V} are of $(hw + h_1 w_1 + h_2 w_2) \times d$ and $(hw + h_1 w_1 + h_2 w_2) \times 2d$, respectively. Following the original attention mechanism, the query tensor \mathbf{Q} , multi-scale key and values tensors \mathbf{K}, \mathbf{V} are sent to compute the output of self-attention

$$\text{Attn}(\mathbf{Q}, \mathbf{K}, \mathbf{V}) = \text{Softmax}\left(\frac{\mathbf{Q}\mathbf{K}^T}{\sqrt{d}}\right) \mathbf{V} \in \mathbb{R}^{hw \times 2d}.\quad (6)$$

As the multi-scale \mathbf{K}, \mathbf{V} are approximate of sizes $(hw + \frac{1}{4}hw + \frac{1}{9}hw) \times d$ and $(hw + \frac{1}{4}hw + \frac{1}{9}hw) \times 2d$, CSA only adds marginal computation cost compared to its single-scale counterpart, whose \mathbf{K}, \mathbf{V} have the sizes of $hw \times d$ and $hw \times 2d$, respectively. The saliency maps in Fig. 1b help demonstrate the benefit of maintaining cross-scale interactions in CSA.

Parallel Convolution Path. The self-attention mechanism in Eq. (6) is often considered poor at distinguishing between long-range and short-range relationships, where structural information [32] and local relationships [47] play a significant role in vision tasks. Accordingly, we incorporate the Parallel Convolution Path (PCP), a technique drawn from HRViT [21], which acts as a relative positional encoding to preserve local information in self-attention. The modified self-attention with PCP now becomes

$$\text{ModifiedAttn}(\mathbf{Q}, \mathbf{K}, \mathbf{V}) = \text{Attn}(\mathbf{Q}, \mathbf{K}, \mathbf{V}) + \text{ConvPath}(\mathbf{V}_0) \in \mathbb{R}^{hw \times 2d}.\quad (7)$$

A detailed description of the PCP is in the Appendix.

3.3 Intra-Feed-Forward Network (Intra-FFN)

The Feed-Forward Network (FFN) is also an essential part of the design of attention blocks. For the FFN, we follow the design in [75, 39, 81, 65] which is a 3×3 depthwise convolution inserted between

Component	FLOPs (G)	Percentage
CSA	0.049	2.1%
FFN	0.081	3.5%
Intra-FFN	0.030	1.3%

Table 1: **FLOPs summary of MSCSA components in PVTv2-B1+MSCSA.** Assuming the input image has a size of 224×224 .

two linear projections, as shown in Fig. 3c. The two linear projections, *i.e.*, 1×1 convolutions, enable feature interaction between stages, while the depthwise convolution acts as another positional encoding layer to supplement the PCP [21] in CSA and to encourage local feature aggregation.

Since the input to the FFN is the multi-stage feature map which usually has a large channel dimension, the two linear projections in FFN carry a massive amount of FLOPs. As shown in Tab. 1, in one MSCSA block, the FLOPs of a single FFN layer is close to two CSA layers. To overcome this issue, we propose our Intra-Feed-Forward Network (Intra-FFN). In the Intra-FFN, the multi-stage feature map is first split into several parts, where the number of parts matches the number of stages in the backbone, and each part has a channel dimension corresponding to its original stage. Then, the feature maps from each of the parts are fed into several FFNs separately, and their outputs are concatenated back into a multi-stage feature map. In the MSCSA block, half of the FFN layers are replaced by Intra-FFN layers, which allows savings in computation. The saved computation by Intra-FFN can be spent on enlarging the channel dimension of the multi-stage feature map and increasing the expansion ratio of linear projections in FFN, which enriches multi-stage interactions. The ablation study in Sec. 4.3 confirms that Intra-FFN in MSCSA leads to a performance gain with a similar computational cost compared to FFN.

3.4 MSCSA and Architectural Variants

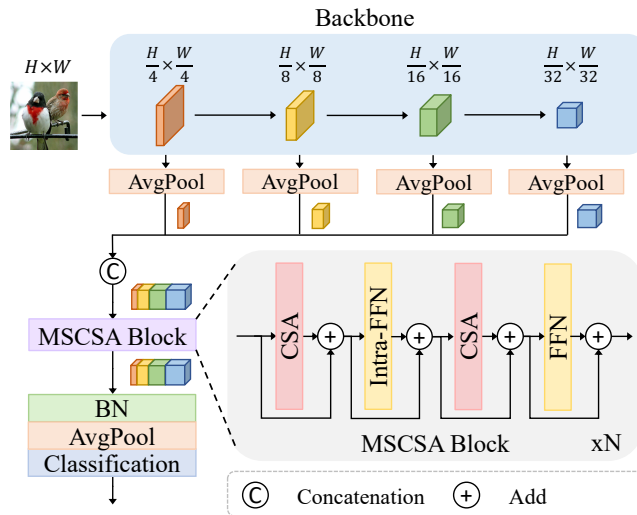


Figure 4: **Multi-Stage Cross-Scale Attention (MSCSA) for classification.** Feature maps from different scales are pooled (with averaging) to the same size. An additional 1×1 convolution layer can be optionally applied to further decrease the number of channels and reduce FLOPs. Afterward, feature maps from all four stages are concatenated along the channel dimension and fed into several MSCSA blocks.

The construction of MSCSA begins by taking inputs from feature maps in different stages of a vision backbone, where the backbone usually has four stages with resolutions from $H/4 \times W/4$ to $H/32 \times W/32$ ¹. Feature maps from different scales are average-pooled to a target size, *e.g.*, $H/32 \times W/32$, to enable efficient feature interactions. Moreover, for backbones with a large number

¹Extending MSCSA to vision backbones with different numbers of stages is straightforward.

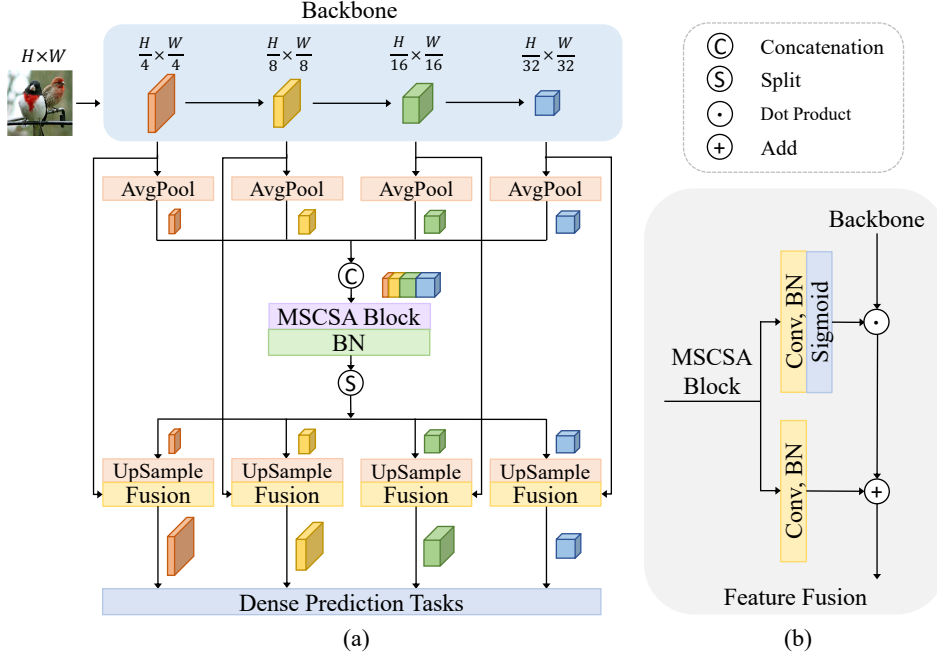


Figure 5: (a) **Multi-Stage Cross-Scale Attention (MSCSA) for dense prediction tasks.** For dense prediction tasks, the multi-stage feature map from MSCSA blocks (same as in Fig. 4) is split into several parts corresponding to the number of channels in each stage and upsampled to their original resolutions. Together with the feature maps from the original backbone, they are fused through feature fusion layers. Finally, the fused feature maps in all scales are fed into downstream networks for dense prediction tasks. (b) **Detailed architecture of feature fusion layer.** The upsampled feature map from MSCSA blocks generate injection weights and biases. Then, the weights and biases are fused with the feature map from the backbone via element-wise multiplication and addition, respectively.

of channels, an additional 1×1 convolution layer will be applied to decrease the channel dimension and further reduce FLOPs. Afterward, feature maps from different stages are concatenated along the channel dimension to obtain a multi-stage feature map. This feature map is then fed into a stack of several MSCSA blocks to apply feature interactions between different stages and scales, where the MSCSA block is a stack of a CSA layer followed by an Intra-FFN layer and another CSA layer followed by an FFN layer. For classification and dense prediction tasks, we provide two architectural variants in Figs. 4 and 5.

4 Experiments

To validate that MSCSA can widely enhance the performance of vision backbones via multi-stage and cross-scale feature map interactions, we implement and evaluate MSCSA on a variety of convolution and attention-based vision backbones. Our baselines include TopFormer [81] and CoaT [70]. These two models have similar multi-stage feature interactions, where TopFormer has a convolution-based backbone, and CoaT has a ViT-based backbone. We substitute the attention modules and the parallel blocks in TopFormer and CoaT with MSCSA, respectively, and match the FLOPs of the corresponding baseline models. Moreover, we test our MSCSA on CNN backbones ResNet [24] and ConvNeXt [45], ViT backbones PVTv2 [65], P2T [67], and Swin [44].

The Cross-Scale Attention (CSA) in Sec. 3.2 is designed to facilitate downstream tasks by introducing interactions between feature maps of different scales. Therefore, we mainly evaluate the performance of our MSCSA integrated with these vision backbones on downstream tasks, including object detection and instance segmentation on the COCO dataset [42] (Sec. 4.1), and semantic segmentation on the ADE20K dataset [83] (Sec. 4.2). For completeness, we also present the performance on image classification on the ImageNet-1k dataset [14] in the Appendix. Finally, we conduct a series of ablation studies in Sec. 4.3 to test the effectiveness of each component of MSCSA.

Method	Backbone	FLOPs (G)	FPS	AP ^b	AP ^b ₅₀	AP ^b ₇₅	AP ^m	AP ^m ₅₀	AP ^m ₇₅
Mask R-CNN	CoaT Tiny*	260	30	42.7	64.7	46.5	38.7	61.7	41.4
	CoaT Tiny+MSCSA	237(-8.8%)	41(+36.7%)	43.9(+1.2)	66.0	48.1	39.8(+1.1)	62.7	42.2
	CoaT Small	428	17	46.5	68.5	51.1	41.8	65.5	45.0
	CoaT Small+MSCSA	318(-25.7%)	31(+82.4%)	46.4(-0.1)	69.2	50.7	42.1(+0.3)	65.7	45.1
	ResNet-50 [†]	260	103	38.2	59.0	41.5	35.4	56.3	37.9
	ResNet-50+MSCSA	271(+4.2%)	86(-18.4%)	42.2(+4.0)	63.8	46.1	38.7(+3.3)	60.8	41.4
	PVTv2-B0	196	62	38.2	60.5	40.7	36.2	57.8	38.6
	PVTv2-B0+MSCSA	199(+1.5%)	59(-4.8%)	41.0(+2.8)	62.8	44.4	37.8(+1.6)	59.9	40.7
	PVTv2-B1	244	47	41.8	64.3	45.9	38.8	61.2	41.6
	PVTv2-B1+MSCSA	250(+2.5%)	44(-6.4%)	43.8(+2.0)	65.6	47.9	40.0(+1.2)	62.6	43.0
	PVTv2-B2	309	28	45.3	67.1	49.6	41.2	64.2	44.4
	PVTv2-B2+MSCSA	322(+4.2%)	27(-3.6%)	46.0(+0.7)	67.7	50.6	41.5(+0.3)	64.8	44.8
	P2T-Tiny	225	44	43.3	65.7	47.3	39.6	62.5	42.3
	P2T-Tiny+MSCSA	232(+3.1%)	41(-6.8%)	44.9(+1.6)	67.0	49.1	40.7(+1.1)	64.2	43.8
Swin-T	267	41	43.7	66.6	47.6	39.8	63.3	42.7	
Swin-T+MSCSA	284(+6.4%)	38(-7.3%)	44.3(+0.6)	66.7	48.5	40.5(+0.7)	63.6	43.4	
ConvNeXt-T*	262	45	43.8	65.8	48.2	40.2	62.9	43.2	
ConvNeXt-T+MSCSA	279 (+6.5%)	42(-6.7%)	45.6(+1.8)	67.8	50.0	41.7(+1.5)	64.9	44.8	
Cascade Mask R-CNN	ResNet-50	394	99	41.2	59.4	45.0	35.9	56.6	38.4
ResNet-50+MSCSA	405(+2.8%)	81(-18.2%)	43.4(+2.2)	62.3	47.2	37.7(+1.8)	59.4	40.6	
Method	Backbone	FLOPs (G)	FPS	AP ^b	AP ^b ₅₀	AP ^b ₇₅	AP ^b _S	AP ^b _M	AP ^b _L
RetinaNet	ResNet-50	239	98	36.5	55.4	39.1	20.4	40.3	48.1
	ResNet-50+MSCSA	253(+5.9%)	80(-18.4%)	39.0(+2.5)	58.9	41.7	23.6	43.0	51.4
Deformable DETR	ResNet-50	173	38	44.5	63.2	48.9	28.0	47.8	58.8
	ResNet-50+MSCSA	185(+6.9%)	34(-10.5%)	45.6(+1.1)	64.7	49.8	27.5	49.0	60.4

Table 2: **COCO object detection and instance segmentation results.** [†] indicates the backbone is re-trained by us. * indicates this reference model is trained by us because it is not provided by the reference. Mask R-CNN [23], Cascade Mask R-CNN [2], and RetinaNet [41] are trained with $1\times$ schedule, while Deformable DETR [84] is trained with 50-epoch schedule. Moreover, CoaT-based models are trained with multi-scale training inputs (MS) [44, 55] following the CoaT [70] training pipeline, while the other models are trained with single-scale training inputs (SS) [44]. FLOPs are computed with an input resolution of 800×1280 . Throughputs are tested on an NVIDIA A100 GPU, and the other settings follow [44].

4.1 Object Detection and Instance Segmentation

Settings To evaluate the capability of vision backbones combined with our MSCSA on object detection and instance segmentation, we conduct experiments on the COCO dataset [42] with MMDetection [4] toolbox, where the feature extractors are vision backbones integrated with MSCSA pretrained on ImageNet-1k. We first evaluate the performance of CoaT [70], ResNet [24], PVTv2 [65], P2T [67], swin [44], and ConvNeXt [45] backbones on Mask R-CNN [23]. Moreover, we test the performance of ResNet-50+MSCSA with other mainstream detectors including Cascade Mask R-CNN [2], RetinaNet [41], and Deformable-DETR [84]. For ResNet ones, we use the default setting for ResNet from MMDetection with some minor changes. For all other backbones, we apply their shared training configurations. In general, all the detection networks except for Deformable DETR are trained for 12 epochs ($1\times$ schedule), while Deformable DETR is trained for 50 epochs. For CoaT-based models, we apply the multi-scale training strategy (MS) [44, 55] following their original settings, while for the other models, we adopt the single-scale one (SS). The detailed training settings are in the Appendix.

Results Tab. 2 summarizes the performance of MSCSA on several backbones. For CoaT, we replace its parallel blocks with MSCSA. CoaT Tiny+MSCSA and CoaT Small+MSCSA achieve better or similar accuracy with smaller FLOPs and significantly reduced runtime. This is because CoaT maintains parallel blocks in different resolutions and requires several rounds of communication between these parallel blocks. Hence, replacing parallel blocks with the lightweight MSCSA leads to improved computation efficiency. For the other vision backbones, MSCSA is applied as an add-on module, boosting their performance with less than 7% additional FLOPs. Other than the CUDA-optimized ResNet50 backbones², the runtime increases in proportion to FLOPs.

²CUDA has specific runtime optimizations on convolutions, which are not available for the matrix multiplications in MSCSA. In Table 2, ResNet-50 with Mask R-CNN has a FLOPs of 260G, which is larger than or similar to the other backbones with Mask R-CNN. However, it has a FPS of 103, which is significantly larger.

Backbone	FLOPs (G)	FPS	mIoU
TopFormer-T [†]	0.55	960	33.6
TopFormer-T+MSCSA	0.55	948(-1.3%)	34.1(+0.5)
TopFormer-B [†]	1.8	578	38.3
TopFormer-B+MSCSA	1.8	585(+1.2%)	38.9(+0.6)
PVTv2-B0	25	305	37.2
PVTv2-B0+MSCSA	26(+4.0%)	285(-6.6%)	40.1(+2.9)
PVTv2-B1	34	225	42.5
PVTv2-B1+MSCSA	36(+5.9%)	205(-8.8%)	44.1(+1.6)
PVTv2-B2	46	146	45.2
PVTv2-B2+MSCSA	49(+6.5%)	132(-9.6%)	46.3(+1.1)

Table 3: **ADE20k semantic segmentation results.** [†] indicates the backbone of this reference model is re-trained by us. For TopFormer-based models, we use the segmentation head proposed by TopFormer [81]. The network is trained for 160k iterations with a batch size of 16. PVTv2-based models are trained with Semantic FPN [33], where the networks are trained for 40k iterations with a batch size of 32 following the shared pipeline. FLOPs are computed with 512×512 resolution.

4.2 Semantic Segmentation

Settings We also test vision backbones integrated with MSCSA on semantic segmentation. We conduct experiments on TopFormer [81] and PVTv2 [65]-based models on the ADE20k dataset [83] with MMSegmentation [11] toolbox, where the backbones are pretrained on ImageNet-1k. For both TopFormer and PVTv2-based models, we use the corresponding training pipelines. And for TopFormer-based models, the segmentation head is the one proposed by TopFormer, whereas for PVTv2-based models, the models are trained with Semantic FPN [33]. Following the configuration of each model, we train TopFormer ones with a mini-batch of 16 images for 160k iterations and PVTv2 ones with a mini-batch of 32 images for 40k iterations. The detailed training settings are in the Appendix.

Results The semantic segmentation results are shown in Tab. 3. For TopFormer backbones, MSCSA replaces their Scale-Aware Semantics Extractor. MSCSA improves mIoU and keeps the FLOPs and FPS to be nearly the same. For PVTv2 backbones, MSCSA boosts the performance of PVTv2-B0/B1/B2 by 2.9%/1.6%/1.1% with less than 10% additional FLOPs and runtime. These results demonstrate the effectiveness of MSCSA as an add-on module on semantic segmentation.

4.3 Ablation Studies

This section describes a series of ablation studies on TopFormer-T [81]+MSCSA on ImageNet-1k [14] to validate the effectiveness of each component in MSCSA.

Setting	FLOPs (M)	FPS	Top-1 Acc.
All opt. removed	129	9437	65.1
+ w. PCP	129(+0)	9254(-1.9%)	65.7(+0.6)
++ w. Intra-FFN	130(+1)	9014(-4.5%)	66.0(+0.9)
+++ w. MSP	132(+3)	8757(-7.2%)	67.1(+2.0)

Table 4: **Component Analysis on TopFormer-T+MSCSA.** We start by removing all the component options from TopFormer-T+MSCSA. And the effectiveness of each major component is evaluated by cumulatively adding each component back.

Effectiveness of MSP, Intra-FFN and PCP [21]. The analysis of the major components is shown in Tab. 4, where the performance is evaluated by first removing all the components and then cumulatively adding each component back. The significant performance improvement comes from the Multi-Scale key, value tensor Projections (MSP) part, which brings about a 1.1% accuracy gain with negligible additional FLOPs. This result confirms that the cross-scale feature interaction by MSP does help the model generalize better. On the other hand, by replacing half of the FFNs with our proposed Intra-FFN, we put more computational budget to increase the expansion ratio of linear projections in FFNs in the case of TopFormer. And this architectural modification gives us about a

Variants	FLOPs (M)	FPS	Top-1 Acc.
TopFormer-T+MSCSA	132	8757	67.1
-/+ AvgPool	132(-0)	8744(-0.1%)	66.7(-0.4)
-/+ Cas. Conv	131(-1)	8802(+0.5%)	66.9(-0.2)
-/+ Sin. Conv	131(-1)	8931(+2.0%)	66.4(-0.7)

Table 5: **Analysis of different down-sampling strategies.** MSCSA is MSCSA in short. The different design choices are illustrated in Fig. 6. The effectiveness of each design choice is evaluated on TopFormer-T+MSCSA by replacing the default setting with the specific design.

0.3% accuracy gain. Moreover, by adding the parallel convolution path (PCP) [21] into the attention module, the top-1 accuracy increases by 0.6%. This result validates the effectiveness of local feature aggregation in PCP.

Effectiveness of different down-sampling strategies in MSP. Since the major contribution of our MSCSA comes from the MSP part. Another series of ablation studies are conducted to evaluate the effectiveness of several down-sampling strategies. As illustrated in Fig. 6, instead of the default setting (Fig. 6a) in MSP, we replace the depthwise convolution with average pooling (Fig. 6b), replace the parallel convolution structure with cascade convolutions (Fig. 6c), and drop the feature map in lowest resolution (Fig. 6d). Benefiting from more trainable parameters, the parallel convolution structure achieves the best performance as shown in Tab. 5, thus becoming our default setting in CSA. The performance gap between the single convolution design and the other three design choices demonstrates the advantage of generating feature maps in three different scales with small additional computational cost.

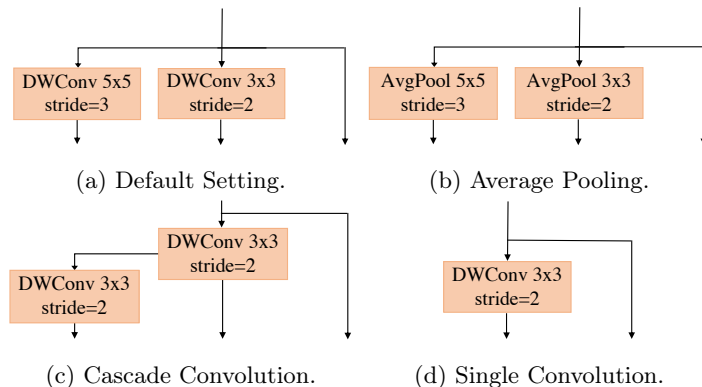


Figure 6: **Different down-sampling strategies.**

5 Conclusion

This work presented an add-on module, Multi-Stage Cross-Scale Attention (MSCSA), to enhance the performance of vision backbones by introducing interactions between feature maps in different stages and objects of different scales. MSCSA works well for various vision backbones and attains a clear performance boost on common benchmark tasks with moderate additional FLOPs and runtime. Future work involves applying MSCSA on additional network architectures suitable for biomedical and neuroimaging tasks such as diffusion MRI pre-processing (e.g., denoising, distortion corrections) and estimation of biophysical and signal models, image registration, image quality transfer, stroke lesion segmentation, multi-modal brain age estimation, classification of disease and cognitive impairment status, prediction of progression to various forms of Alzheimer’s and related dementias (ADRDs) such as the vascular contributions to cognitive impairments and dementia (VCID).

6 Acknowledgement

We would like to acknowledge the support from NIH grants R01NS123378, P50HD105353, NIH R01NS105646, NIH R01NS11102, and R01NS117568.

References

- [1] Jimmy Lei Ba, Jamie Ryan Kiros, and Geoffrey E Hinton. Layer normalization. *arXiv preprint arXiv:1607.06450*, 2016.
- [2] Zhaowei Cai and Nuno Vasconcelos. Cascade r-cnn: high quality object detection and instance segmentation. *IEEE transactions on pattern analysis and machine intelligence*, 43(5):1483–1498, 2019.
- [3] Chun-Fu Richard Chen, Quanfu Fan, and Rameswar Panda. Crossvit: Cross-attention multi-scale vision transformer for image classification. In *Proceedings of the IEEE/CVF international conference on computer vision*, pages 357–366, 2021.
- [4] Kai Chen, Jiaqi Wang, Jiangmiao Pang, Yuhang Cao, Yu Xiong, Xiaoxiao Li, Shuyang Sun, Wansen Feng, Ziwei Liu, Jiarui Xu, Zheng Zhang, Dazhi Cheng, Chenchen Zhu, Tianheng Cheng, Qijie Zhao, Buyu Li, Xin Lu, Rui Zhu, Yue Wu, Jifeng Dai, Jingdong Wang, Jianping Shi, Wanli Ouyang, Chen Change Loy, and Dahua Lin. MMDetection: Open mmlab detection toolbox and benchmark. *arXiv preprint arXiv:1906.07155*, 2019.
- [5] Liang-Chieh Chen, George Papandreou, Iasonas Kokkinos, Kevin Murphy, and Alan L Yuille. Deeplab: Semantic image segmentation with deep convolutional nets, atrous convolution, and fully connected crfs. *IEEE transactions on pattern analysis and machine intelligence*, 40(4):834–848, 2017.
- [6] Qiang Chen, Qiman Wu, Jian Wang, Qinghao Hu, Tao Hu, Errui Ding, Jian Cheng, and Jingdong Wang. Mixformer: Mixing features across windows and dimensions. In *Proceedings of the IEEE/CVF Conference on Computer Vision and Pattern Recognition*, pages 5249–5259, 2022.
- [7] Zhengsu Chen, Lingxi Xie, Jianwei Niu, Xuefeng Liu, Longhui Wei, and Qi Tian. Visformer: The vision-friendly transformer. In *Proceedings of the IEEE/CVF International Conference on Computer Vision*, pages 589–598, 2021.
- [8] Zhiyang Chen, Yousong Zhu, Chaoyang Zhao, Guosheng Hu, Wei Zeng, Jinqiao Wang, and Ming Tang. Dpt: Deformable patch-based transformer for visual recognition. In *Proceedings of the 29th ACM International Conference on Multimedia*, pages 2899–2907, 2021.
- [9] Xiangxiang Chu, Zhi Tian, Yuqing Wang, Bo Zhang, Haibing Ren, Xiaolin Wei, Huaxia Xia, and Chunhua Shen. Twins: Revisiting the design of spatial attention in vision transformers. *Advances in Neural Information Processing Systems*, 34:9355–9366, 2021.
- [10] MMCV Contributors. MMCV: OpenMMLab computer vision foundation. <https://github.com/open-mmlab/mmcv>.
- [11] MMSegmentation Contributors. MMSegmentation: Openmmlab semantic segmentation toolbox and benchmark. <https://github.com/open-mmlab/mms Segmentation>, 2020.
- [12] Timm Contributors. Pytorch image models (timm). <https://github.com/fastai/timmdocs>.
- [13] Ekin D Cubuk, Barret Zoph, Dandelion Mane, Vijay Vasudevan, and Quoc V Le. Autoaugment: Learning augmentation policies from data. *arXiv preprint arXiv:1805.09501*, 2018.
- [14] Jia Deng, Wei Dong, Richard Socher, Li-Jia Li, Kai Li, and Li Fei-Fei. Imagenet: A large-scale hierarchical image database. In *2009 IEEE conference on computer vision and pattern recognition*, pages 248–255. Ieee, 2009.
- [15] Jacob Devlin, Ming-Wei Chang, Kenton Lee, and Kristina Toutanova. Bert: Pre-training of deep bidirectional transformers for language understanding. *arXiv preprint arXiv:1810.04805*, 2018.

- [16] Xiaoyi Dong, Jianmin Bao, Dongdong Chen, Weiming Zhang, Nenghai Yu, Lu Yuan, Dong Chen, and Baining Guo. Cswin transformer: A general vision transformer backbone with cross-shaped windows. In *Proceedings of the IEEE/CVF Conference on Computer Vision and Pattern Recognition*, pages 12124–12134, 2022.
- [17] Alexey Dosovitskiy, Lucas Beyer, Alexander Kolesnikov, Dirk Weissenborn, Xiaohua Zhai, Thomas Unterthiner, Mostafa Dehghani, Matthias Minderer, Georg Heigold, Sylvain Gelly, et al. An image is worth 16x16 words: Transformers for image recognition at scale. *arXiv preprint arXiv:2010.11929*, 2020.
- [18] Haoqi Fan, Bo Xiong, Karttikeya Mangalam, Yanghao Li, Zhicheng Yan, Jitendra Malik, and Christoph Feichtenhofer. Multiscale vision transformers. In *Proceedings of the IEEE/CVF International Conference on Computer Vision*, pages 6824–6835, 2021.
- [19] Shang-Hua Gao, Ming-Ming Cheng, Kai Zhao, Xin-Yu Zhang, Ming-Hsuan Yang, and Philip Torr. Res2net: A new multi-scale backbone architecture. *IEEE transactions on pattern analysis and machine intelligence*, 43(2):652–662, 2019.
- [20] Benjamin Graham, Alaaeldin El-Nouby, Hugo Touvron, Pierre Stock, Armand Joulin, Hervé Jégou, and Matthijs Douze. Levit: a vision transformer in convnet’s clothing for faster inference. In *Proceedings of the IEEE/CVF international conference on computer vision*, pages 12259–12269, 2021.
- [21] Jiaqi Gu, Hyoukjun Kwon, Dilin Wang, Wei Ye, Meng Li, Yu-Hsin Chen, Liangzhen Lai, Vikas Chandra, and David Z Pan. Multi-scale high-resolution vision transformer for semantic segmentation. In *Proceedings of the IEEE/CVF Conference on Computer Vision and Pattern Recognition*, pages 12094–12103, 2022.
- [22] Ali Hassani, Steven Walton, Jiachen Li, Shen Li, and Humphrey Shi. Neighborhood attention transformer. *arXiv preprint arXiv:2204.07143*, 2022.
- [23] Kaiming He, Georgia Gkioxari, Piotr Dollár, and Ross Girshick. Mask r-cnn. In *Proceedings of the IEEE international conference on computer vision*, pages 2961–2969, 2017.
- [24] Kaiming He, Xiangyu Zhang, Shaoqing Ren, and Jian Sun. Deep residual learning for image recognition. In *Proceedings of the IEEE conference on computer vision and pattern recognition*, pages 770–778, 2016.
- [25] Geoffrey Hinton. Neural networks for machine learning. http://www.cs.toronto.edu/~tijmen/csc321/slides/lecture_slides_lec6.pdf.
- [26] Elad Hoffer, Tal Ben-Nun, Itay Hubara, Niv Giladi, Torsten Hoefer, and Daniel Soudry. Augment your batch: Improving generalization through instance repetition. In *Proceedings of the IEEE/CVF Conference on Computer Vision and Pattern Recognition*, pages 8129–8138, 2020.
- [27] Andrew Howard, Mark Sandler, Grace Chu, Liang-Chieh Chen, Bo Chen, Mingxing Tan, Weijun Wang, Yukun Zhu, Ruoming Pang, Vijay Vasudevan, et al. Searching for mobilenetv3. In *Proceedings of the IEEE/CVF international conference on computer vision*, pages 1314–1324, 2019.
- [28] Gao Huang, Zhuang Liu, Laurens Van Der Maaten, and Kilian Q Weinberger. Densely connected convolutional networks. In *Proceedings of the IEEE conference on computer vision and pattern recognition*, pages 4700–4708, 2017.
- [29] Gao Huang, Yu Sun, Zhuang Liu, Daniel Sedra, and Kilian Q Weinberger. Deep networks with stochastic depth. In *European conference on computer vision*, pages 646–661. Springer, 2016.
- [30] Zilong Huang, Youcheng Ben, Guozhong Luo, Pei Cheng, Gang Yu, and Bin Fu. Shuffle transformer: Rethinking spatial shuffle for vision transformer. *arXiv preprint arXiv:2106.03650*, 2021.
- [31] Sergey Ioffe and Christian Szegedy. Batch normalization: Accelerating deep network training by reducing internal covariate shift. In *International conference on machine learning*, pages 448–456. PMLR, 2015.

- [32] Md Amirul Islam, Sen Jia, and Neil DB Bruce. How much position information do convolutional neural networks encode? *arXiv preprint arXiv:2001.08248*, 2020.
- [33] Alexander Kirillov, Ross Girshick, Kaiming He, and Piotr Dollár. Panoptic feature pyramid networks. In *Proceedings of the IEEE/CVF conference on computer vision and pattern recognition*, pages 6399–6408, 2019.
- [34] Alex Krizhevsky, Ilya Sutskever, and Geoffrey E Hinton. Imagenet classification with deep convolutional neural networks. *Communications of the ACM*, 60(6):84–90, 2017.
- [35] Gustav Larsson, Michael Maire, and Gregory Shakhnarovich. Fractalnet: Ultra-deep neural networks without residuals. *arXiv preprint arXiv:1605.07648*, 2016.
- [36] Youngwan Lee, Jonghee Kim, Jeffrey Willette, and Sung Ju Hwang. Mpvit: Multi-path vision transformer for dense prediction. In *Proceedings of the IEEE/CVF Conference on Computer Vision and Pattern Recognition*, pages 7287–7296, 2022.
- [37] Jinpeng Li, Yichao Yan, Shengcai Liao, Xiaokang Yang, and Ling Shao. Local-to-global self-attention in vision transformers. *arXiv preprint arXiv:2107.04735*, 2021.
- [38] Yanghao Li, Chao-Yuan Wu, Haoqi Fan, Karttikeya Mangalam, Bo Xiong, Jitendra Malik, and Christoph Feichtenhofer. Mvitv2: Improved multiscale vision transformers for classification and detection. In *Proceedings of the IEEE/CVF Conference on Computer Vision and Pattern Recognition*, pages 4804–4814, 2022.
- [39] Yawei Li, Kai Zhang, Jiezhong Cao, Radu Timofte, and Luc Van Gool. Localvit: Bringing locality to vision transformers. *arXiv preprint arXiv:2104.05707*, 2021.
- [40] Hezheng Lin, Xing Cheng, Xiangyu Wu, and Dong Shen. Cat: Cross attention in vision transformer. In *2022 IEEE International Conference on Multimedia and Expo (ICME)*, pages 1–6. IEEE, 2022.
- [41] Tsung-Yi Lin, Priya Goyal, Ross Girshick, Kaiming He, and Piotr Dollár. Focal loss for dense object detection. In *Proceedings of the IEEE international conference on computer vision*, pages 2980–2988, 2017.
- [42] Tsung-Yi Lin, Michael Maire, Serge Belongie, James Hays, Pietro Perona, Deva Ramanan, Piotr Dollár, and C Lawrence Zitnick. Microsoft coco: Common objects in context. In *European conference on computer vision*, pages 740–755. Springer, 2014.
- [43] Fang Liu, Bochen Guan, Zhaoye Zhou, Alexey Samsonov, Humberto Rosas, Kevin Lian, Ruchi Sharma, Andrew Kanarek, John Kim, Ali Guermazi, et al. Fully automated diagnosis of anterior cruciate ligament tears on knee mr images by using deep learning. *Radiology. Artificial intelligence*, 1(3), 2019.
- [44] Ze Liu, Yutong Lin, Yue Cao, Han Hu, Yixuan Wei, Zheng Zhang, Stephen Lin, and Baining Guo. Swin transformer: Hierarchical vision transformer using shifted windows. In *Proceedings of the IEEE/CVF International Conference on Computer Vision*, pages 10012–10022, 2021.
- [45] Zhuang Liu, Hanzi Mao, Chao-Yuan Wu, Christoph Feichtenhofer, Trevor Darrell, and Saining Xie. A convnet for the 2020s. *Proceedings of the IEEE/CVF Conference on Computer Vision and Pattern Recognition (CVPR)*, 2022.
- [46] Ilya Loshchilov and Frank Hutter. Decoupled weight decay regularization. *arXiv preprint arXiv:1711.05101*, 2017.
- [47] David G Lowe. Object recognition from local scale-invariant features. In *Proceedings of the seventh IEEE international conference on computer vision*, volume 2, pages 1150–1157. Ieee, 1999.
- [48] Junting Pan, Adrian Bulat, Fuwen Tan, Xiatian Zhu, Lukasz Dudziak, Hongsheng Li, Georgios Tzimiropoulos, and Brais Martinez. Edgevits: Competing light-weight cnns on mobile devices with vision transformers. In *European Conference on Computer Vision*, pages 294–311. Springer, 2022.

- [49] Adam Paszke, Sam Gross, Francisco Massa, Adam Lerer, James Bradbury, Gregory Chanan, Trevor Killeen, Zeming Lin, Natalia Gimelshein, Luca Antiga, et al. Pytorch: An imperative style, high-performance deep learning library. *Advances in neural information processing systems*, 32, 2019.
- [50] Pengzhen Ren, Changlin Li, Guangrun Wang, Yun Xiao, Qing Du, Xiaodan Liang, and Xiaojun Chang. Beyond fixation: Dynamic window visual transformer. In *Proceedings of the IEEE/CVF Conference on Computer Vision and Pattern Recognition*, pages 11987–11997, 2022.
- [51] Sucheng Ren, Daquan Zhou, Shengfeng He, Jiashi Feng, and Xinchao Wang. Shunted self-attention via multi-scale token aggregation. In *Proceedings of the IEEE/CVF Conference on Computer Vision and Pattern Recognition*, pages 10853–10862, 2022.
- [52] Fahad Shamshad, Salman Khan, Syed Waqas Zamir, Muhammad Haris Khan, Munawar Hayat, Fahad Shahbaz Khan, and Huazhu Fu. Transformers in medical imaging: A survey. *arXiv preprint arXiv:2201.09873*, 2022.
- [53] Karen Simonyan and Andrew Zisserman. Two-stream convolutional networks for action recognition in videos. *Advances in neural information processing systems*, 27, 2014.
- [54] Karen Simonyan and Andrew Zisserman. Very deep convolutional networks for large-scale image recognition. *arXiv preprint arXiv:1409.1556*, 2014.
- [55] Peize Sun, Rufeng Zhang, Yi Jiang, Tao Kong, Chenfeng Xu, Wei Zhan, Masayoshi Tomizuka, Lei Li, Zehuan Yuan, Changhu Wang, et al. Sparse r-cnn: End-to-end object detection with learnable proposals. In *Proceedings of the IEEE/CVF conference on computer vision and pattern recognition*, pages 14454–14463, 2021.
- [56] Christian Szegedy, Sergey Ioffe, Vincent Vanhoucke, and Alexander A Alemi. Inception-v4, inception-resnet and the impact of residual connections on learning. In *Thirty-first AAAI conference on artificial intelligence*, 2017.
- [57] Christian Szegedy, Wei Liu, Yangqing Jia, Pierre Sermanet, Scott Reed, Dragomir Anguelov, Dumitru Erhan, Vincent Vanhoucke, and Andrew Rabinovich. Going deeper with convolutions. In *Proceedings of the IEEE conference on computer vision and pattern recognition*, pages 1–9, 2015.
- [58] Christian Szegedy, Vincent Vanhoucke, Sergey Ioffe, Jon Shlens, and Zbigniew Wojna. Rethinking the inception architecture for computer vision. In *Proceedings of the IEEE conference on computer vision and pattern recognition*, pages 2818–2826, 2016.
- [59] Hugo Touvron, Matthieu Cord, Matthijs Douze, Francisco Massa, Alexandre Sablayrolles, and Hervé Jégou. Training data-efficient image transformers & distillation through attention. In *International Conference on Machine Learning*, pages 10347–10357. PMLR, 2021.
- [60] Zhengzhong Tu, Hossein Talebi, Han Zhang, Feng Yang, Peyman Milanfar, Alan Bovik, and Yinxiao Li. Maxvit: Multi-axis vision transformer. *arXiv preprint arXiv:2204.01697*, 2022.
- [61] Ashish Vaswani, Noam Shazeer, Niki Parmar, Jakob Uszkoreit, Llion Jones, Aidan N Gomez, Łukasz Kaiser, and Illia Polosukhin. Attention is all you need. *Advances in neural information processing systems*, 30, 2017.
- [62] Jingdong Wang, Ke Sun, Tianheng Cheng, Borui Jiang, Chaorui Deng, Yang Zhao, Dong Liu, Yadong Mu, Mingkui Tan, Xinggang Wang, et al. Deep high-resolution representation learning for visual recognition. *IEEE transactions on pattern analysis and machine intelligence*, 43(10):3349–3364, 2020.
- [63] Qiang Wang, Bei Li, Tong Xiao, Jingbo Zhu, Changliang Li, Derek F Wong, and Lidia S Chao. Learning deep transformer models for machine translation. *arXiv preprint arXiv:1906.01787*, 2019.
- [64] Wenhai Wang, Enze Xie, Xiang Li, Deng-Ping Fan, Kaitao Song, Ding Liang, Tong Lu, Ping Luo, and Ling Shao. Pyramid vision transformer: A versatile backbone for dense prediction without convolutions. In *Proceedings of the IEEE/CVF International Conference on Computer Vision*, pages 568–578, 2021.

- [65] Wenhai Wang, Enze Xie, Xiang Li, Deng-Ping Fan, Kaitao Song, Ding Liang, Tong Lu, Ping Luo, and Ling Shao. Pvt v2: Improved baselines with pyramid vision transformer. *Computational Visual Media*, 8(3):415–424, 2022.
- [66] Wenxiao Wang, Lu Yao, Long Chen, Binbin Lin, Deng Cai, Xiaofei He, and Wei Liu. Crossformer: A versatile vision transformer hinging on cross-scale attention. *arXiv preprint arXiv:2108.00154*, 2021.
- [67] Yu-Huan Wu, Yun Liu, Xin Zhan, and Ming-Ming Cheng. P2t: Pyramid pooling transformer for scene understanding. *IEEE Transactions on Pattern Analysis and Machine Intelligence*, 2022.
- [68] Zhuofan Xia, Xuran Pan, Shiji Song, Li Erran Li, and Gao Huang. Vision transformer with deformable attention. In *Proceedings of the IEEE/CVF Conference on Computer Vision and Pattern Recognition*, pages 4794–4803, 2022.
- [69] Enze Xie, Wenhai Wang, Zhiding Yu, Anima Anandkumar, Jose M Alvarez, and Ping Luo. Segformer: Simple and efficient design for semantic segmentation with transformers. *Advances in Neural Information Processing Systems*, 34:12077–12090, 2021.
- [70] Weijian Xu, Yifan Xu, Tyler Chang, and Zhuowen Tu. Co-scale conv-attentional image transformers. In *Proceedings of the IEEE/CVF International Conference on Computer Vision*, pages 9981–9990, 2021.
- [71] Chenglin Yang, Yilin Wang, Jianming Zhang, He Zhang, Zijun Wei, Zhe Lin, and Alan Yuille. Lite vision transformer with enhanced self-attention. In *Proceedings of the IEEE/CVF Conference on Computer Vision and Pattern Recognition*, pages 11998–12008, 2022.
- [72] Jianwei Yang, Chunyuan Li, Pengchuan Zhang, Xiyang Dai, Bin Xiao, Lu Yuan, and Jianfeng Gao. Focal attention for long-range interactions in vision transformers. *Advances in Neural Information Processing Systems*, 34:30008–30022, 2021.
- [73] Rui Yang, Hailong Ma, Jie Wu, Yansong Tang, Xuefeng Xiao, Min Zheng, and Xiu Li. Scalablevit: Rethinking the context-oriented generalization of vision transformer. *arXiv preprint arXiv:2203.10790*, 2022.
- [74] Qihang Yu, Yingda Xia, Yutong Bai, Yongyi Lu, Alan L Yuille, and Wei Shen. Glance-and-gaze vision transformer. *Advances in Neural Information Processing Systems*, 34:12992–13003, 2021.
- [75] Kun Yuan, Shaopeng Guo, Ziwei Liu, Aojun Zhou, Fengwei Yu, and Wei Wu. Incorporating convolution designs into visual transformers. In *Proceedings of the IEEE/CVF International Conference on Computer Vision*, pages 579–588, 2021.
- [76] Yuhui Yuan, Rao Fu, Lang Huang, Weihong Lin, Chao Zhang, Xilin Chen, and Jingdong Wang. Hrformer: High-resolution vision transformer for dense predict. *Advances in Neural Information Processing Systems*, 34:7281–7293, 2021.
- [77] Sangdoon Yun, Dongyoon Han, Seong Joon Oh, Sanghyuk Chun, Junsuk Choe, and Youngjoon Yoo. Cutmix: Regularization strategy to train strong classifiers with localizable features. In *Proceedings of the IEEE/CVF international conference on computer vision*, pages 6023–6032, 2019.
- [78] Cheng Zhang, Haocheng Wan, Xinyi Shen, and Zizhao Wu. Patchformer: An efficient point transformer with patch attention. In *Proceedings of the IEEE/CVF Conference on Computer Vision and Pattern Recognition*, pages 11799–11808, 2022.
- [79] Hongyi Zhang, Moustapha Cisse, Yann N Dauphin, and David Lopez-Paz. mixup: Beyond empirical risk minimization. *arXiv preprint arXiv:1710.09412*, 2017.
- [80] Pengchuan Zhang, Xiyang Dai, Jianwei Yang, Bin Xiao, Lu Yuan, Lei Zhang, and Jianfeng Gao. Multi-scale vision longformer: A new vision transformer for high-resolution image encoding. In *Proceedings of the IEEE/CVF International Conference on Computer Vision*, pages 2998–3008, 2021.

- [81] Wenqiang Zhang, Zilong Huang, Guozhong Luo, Tao Chen, Xinggang Wang, Wenyu Liu, Gang Yu, and Chunhua Shen. Topformer: Token pyramid transformer for mobile semantic segmentation. In *Proceedings of the IEEE/CVF Conference on Computer Vision and Pattern Recognition*, pages 12083–12093, 2022.
- [82] Zhun Zhong, Liang Zheng, Guoliang Kang, Shaozi Li, and Yi Yang. Random erasing data augmentation. In *Proceedings of the AAAI conference on artificial intelligence*, volume 34, pages 13001–13008, 2020.
- [83] Bolei Zhou, Hang Zhao, Xavier Puig, Sanja Fidler, Adela Barriuso, and Antonio Torralba. Scene parsing through ade20k dataset. In *Proceedings of the IEEE conference on computer vision and pattern recognition*, pages 633–641, 2017.
- [84] Xizhou Zhu, Weijie Su, Lewei Lu, Bin Li, Xiaogang Wang, and Jifeng Dai. Deformable detr: Deformable transformers for end-to-end object detection. *arXiv preprint arXiv:2010.04159*, 2020.

A Image Classification

Settings The performance on image classification is evaluated on MSCSA with TopFormer [81], CoaT [70], ResNet [24], PVTv2 [65], P2T [67], Shunted [51], Swin [44], and ConvNeXt [45] on the ImageNet-1k dataset [14], where the implementation is based on PyTorch [49] with MMCV [10] and Timm [12]. For a fair comparison, for CoaT, PVTv2, P2T, Shunted, Swin, and ConvNeXt backbones, we follow the same training pipelines as in their works. For the ResNet backbones, we adopt the training pipeline from PVTv2. Since TopFormer does not release their code for the training pipeline, we choose one from MobileNetV3 [27], which is our best effort in reproducing their results. The detailed training settings are in Appendix C.1.

Model	FLOPs (G)	FPS	Top-1 Acc.
TopFormer-T [†]	0.13	9437	65.1
TopFormer-T+MSCSA	0.13	8757	67.1(+2.0)
TopFormer-B [†]	0.38	6746	75.0
TopFormer-B+MSCSA	0.38	5950	75.5(+0.5)
CoaT Tiny	4.4	120	78.3
CoaT Tiny+MSCSA	4.4	432	81.1(+2.8)
CoaT Small	13	301	82.1
CoaT Small+MSCSA	13	855	83.0(+0.9)
ResNet-50 [†]	4.1	2404	78.3
ResNet-50+MSCSA	4.6	2050	79.9(+1.6)
PVTv2-B0	0.57	3797	70.5
PVTv2-B0+MSCSA	0.65	3479	74.6(+4.1)
PVTv2-B1	2.1	2492	78.7
PVTv2-B1+MSCSA	2.3	2262	80.0(+1.3)
P2T-Tiny	1.8	2087	79.8
P2T-Tiny+MSCSA	2.0	1957	80.9(+1.1)
Shunted-T	2.1	2103	79.8
Shunted-T+MSCSA	2.3	1934	81.0(+1.2)
Swin-T	4.4	1578	81.3
Swin-T+MSCSA	5.0	1414	81.5(+0.2)
ConvNeXt-T	4.5	1955	82.1
ConvNeXt-T+MSCSA	5.1	1732	82.0(-0.1)

Table 6: **ImageNet-1k classification results.** [†] indicates this reference model is re-trained by us. For TopFormer, we substitute the Scale-Aware Semantics Extractor with MSCSA. For CoaT, the parallel blocks are replaced by MSCSA. For all other backbones, MSCSA is added in parallel to the backbones. For TopFormer and CoaT, we match the FLOPs of the corresponding reference model. For all other models, we set the FLOPs cap of MSCSA to be around 10% of the corresponding backbone. All models are trained with 224×224 resolution.

Results The evaluation results of vision backbones combined with our MSCSA are summarized in Tab. 6. For TopFormer and CoaT, we replace their Scale-Aware Semantics Extractor and parallel

Backbone	Pooling Size	Squeeze Ratio	Depth	#Heads	Head Dimension	MLP Ratio
TopFormer-T [81]	1/32 (1/64)	-	2	4	14	3
TopFormer-B [81]	1/32 (1/64)	-	2	8	12	3
CoaT Tiny [70]	1/16 (1/32)	-	3	8	22	1.5
CoaT Small [70]	1/16 (1/32)	-	3	8	52	2
ResNet-18 [24]	1/32	5/8	1	8	24	2
ResNet-50 [24]	1/32	1/4	1	8	32	2
PVTv2-B0 [65]	1/32	3/4	1	8	15	2
PVTv2-B1 [65]	1/32	5/8	1	8	24	2
PVTv2-B2 [65]	1/32	-	1	8	35	2
P2T-Tiny [67]	1/32	3/4	1	8	36	2
Shunted-T [51]	1/32	5/8	1	8	30	2
Swin-T [44]	1/32	3/4	1	12	28	2
ConvNeXt-T [45]	1/32	3/4	1	12	28	2

Table 7: **Model configuration for different backbones.** For TopFormer, we replace the Scale-Aware Semantics Extractor with MSCSA. For CoaT, the Parallel Blocks are replaced by MSCSA. For all other backbones, MSCSA is added in parallel to the backbones. The pooling size for TopFormer follows the size used in ImageNet pre-training, while the value in parentheses is the size used in dense prediction tasks. For CoaT, we also use different pooling sizes for different tasks due to computational constraints. The dimension of value tensors (head dimension) is doubled from those of the query and key tensors, following LeViT [20].

blocks with our MSCSA, respectively. TopFormer+MSCSA and CoaT+MSCSA significantly surpass their corresponding baseline models with similar FLOPs. For CoaT, it maintains parallel blocks in different resolutions and requires several rounds of communication between these parallel blocks, while CoaT+MSCSA replaces parallel blocks with MSCSA, leading to a much smaller runtime. For TopFormer backbones, the runtime is 7-8% slower, likely due to increased memory usage in CSA and Intra-FFN. We believe that better optimizations in the parallel computations of CSA and Intra-FFN can resolve this.

We apply MSCSA as an add-on module to CNN-based ResNet and ConvNeXt and ViT-based PVTv2, P2T, Shunted, and Swin backbones with moderate additional FLOPs and runtime (around 15%). MSCSA successfully boosts the performance of both CNN and ViT backbones. For Swin-T and ConvNeXt-T, MSCSA does not affect the accuracy too much. However, as demonstrated in Tab. 2, MSCSA brings a clear performance improvement on downstream tasks with Swin-T and ConvNeXt-T.

B Model Configuration

To validate that our Multi-Stage Cross-Scale Attention (MSCSA) can enhance the performance of a wide variety of vision backbones via multi-stage and cross-attention feature map interactions, we implement and evaluate MSCSA on several convolution-based and attention-based vision backbones. Our baselines include TopFormer [81] and CoaT [70], which have similar multi-stage feature interactions, where TopFormer has a convolution-based backbone, and CoaT has an attention-based backbone. We replace their attention modules and parallel blocks with MSCSA, respectively. Moreover, we test MSCSA on the well-known CNN backbone ResNet [24] and ConvNeXt [45] and ViT backbone PVTv2 [65], P2T [67], Shunted [51], and Swin [44] to explore the performance gain of MSCSA within a preset complexity cap, *i.e.*, with an increase of approximately 10% of the FLOPs of the backbone. Detailed model configurations are shown in Tab. 7. Parameters in the various configurations are:

- Pooling Size: target pooling size at the beginning of MSCSA
- Squeeze Ratio: channel reduction ratio at the beginning of MSCSA, if applicable.
- Depth: number of MSCSA blocks used in MSCSA.

- #Heads: number of heads in CSA.
- Head Dimension: feature dimension of the query and key tensors in each head.
- MLP Ratio: the expansion ratio in FFN.

C Detailed Training Settings

C.1 ImageNet Classification

Implementation. All the models for ImageNet classification are implemented based on PyTorch [49] with MMCV [10] and Timm [12].

PVTv2 [65] and ResNet [24]. We adopt the shared training pipeline from PVTv2³ and DeiT [59] for PVTv2 and ResNet-based models, where the data augmentations include random cropping [34], random horizontal flipping [34], color jittering [34], label smoothing [58], random erasing [82], repeated augmentation [26], AutoAugmentation [13], Mixup [79], and CutMix [77]. Moreover, the stochastic depth drop [29] is also applied to MSCSA in PVTv2 and ResNet-based models. The models are trained for 300 epochs using AdamW [46] as the optimizer, with a weight decay of 0.05, a mini-batch of 1024 images, an initial learning rate of 0.001, 5 warm-up epochs, and a scaled cosine decay learning ratio scheduler.

CoaT [70]. We adopt the shared training pipeline from CoaT⁴ and DeiT [59] for CoaT-based models, where the data augmentations are identical to the ones used in PVTv2. Moreover, DropPath [35] is applied to MSCSA in CoaT-based models following the design of parallel blocks in CoaT. The models are trained for 300 epochs using AdamW [46] as the optimizer, with a weight decay of 0.05, and a scaled cosine decay learning ratio scheduler. Furthermore, CoaT Tiny+MSCSA is trained with a mini-batch of 2048 images, an initial learning rate of 0.002, 5 warm-up epochs, and exponential moving average (EMA), while CoaT Small+MSCSA is trained with a mini-batch of 1024 images, an initial learning rate of 0.001, and 20 warm-up epochs.

TopFormer [81]. Since TopFormer has not released their code for the training pipeline at the time of this submission, we choose one from MobileNetV3 [27] and Timm⁵ [12], which is our best effort in reproducing their image classification results. The data augmentations are of the same types as the ones used in PVTv2 and CoaT, but with some minor differences in numerical values. The stochastic depth drop [29] is applied to MSCSA following the design of the Scale-Aware Semantics Extractor in TopFormer. The model is trained for 600 epochs with RMSProp [25] as the optimizer, a weight decay of 1e-5, a mini-batch of 1024 images, 3 warm-up epochs, an initial learning rate of 0.064, a step learning rate scheduler with a decay epoch of 2.4, and EMA.

P2T [67]. We adopt the shared training pipeline from P2T⁶ and DeiT [59] for P2T-based models, where the data augmentations are identical to the ones used in PVTv2. And the stochastic depth drop [29] is also applied to MSCSA in P2T-based models. The models are trained for 300 epochs using AdamW [46] as the optimizer, with a weight decay of 0.05, a mini-batch of 1024 images, an initial learning rate of 0.001, 20 warm-up epochs, and a scaled cosine decay learning ratio scheduler.

Shunted [51]. We adopt the shared training pipeline from Shunted⁷ and DeiT [59] for Shunted-based models, where the data augmentations are identical to the ones used in PVTv2. And the stochastic depth drop [29] is also applied to MSCSA in Shunted-based models. The models are trained for 300 epochs using AdamW [46] as the optimizer, with a weight decay of 0.05, a mini-batch of 1024 images, an initial learning rate of 0.001, 5 warm-up epochs, and a scaled cosine decay learning ratio scheduler.

Swin [44]. We adopt the shared training pipeline from Swin⁸ and DeiT [59] for Swin-based models, where the data augmentations are identical to the ones used in PVTv2. And the stochastic depth drop [29] is also applied to MSCSA in Swin-based models. The models are trained for 300 epochs using AdamW [46] as the optimizer, with a weight decay of 0.05, a mini-batch of 1024 images, an initial learning rate of 0.001, 20 warm-up epochs, and a scaled cosine decay learning ratio scheduler.

ConvNeXt [45]. We adopt the shared training pipeline from Swin⁹ and DeiT [59] for ConvNeXt-based models, where the data augmentations are identical to the ones used in PVTv2. And the

³<https://github.com/whai362/PVT>

⁴<https://github.com/mlpc-ucsd/CoaT>

⁵https://huggingface.co/docs/timm/training_hparam_examples

⁶<https://github.com/yuhuan-wu/P2T>

⁷<https://github.com/OliverRensu/Shunted-Transformer>

⁸<https://github.com/microsoft/Swin-Transformer>

⁹<https://github.com/facebookresearch/ConvNeXt>

stochastic depth drop [29] is also applied to MSCSA in ConvNeXt-based models. The models are trained for 300 epochs using AdamW [46] as the optimizer, with a weight decay of 0.05, a mini-batch of 1024 images, an initial learning rate of 0.001, 20 warm-up epochs, and a scaled cosine decay learning ratio scheduler.

C.2 COCO Detection and Instance Segmentation

Implementation. All the models for COCO detection and instance segmentation are implemented based on MMDetection [4].

Mask R-CNN [23]. For CoaT [70], PVTv2 [65], and P2T [67]-based backbones, the detectors are trained with their shared training pipeline. For ResNet [24]-based backbones, the networks are trained with the default Mask R-CNN pipeline from the MMDetection [4] toolbox. Specifically, we adopt the $1\times$ schedule (12 epochs) to train all the models, which decreases the learning rate by $10\times$ after epochs 8 and 11. While all the models use AdamW [46] as the optimizer with a mini-batch of 16 images and 500 linear warm-up iterations, CoaT-based models start with an initial learning rate of 0.0001 and a weight decay of 0.05, PVTv2 and ResNet-based models are trained with an initial learning rate of 0.0002 and a weight decay of 0.0001, and P2T-based models is trained with an initial learning rate of 0.0001 and a weight decay of 0.0001. Moreover, CoaT-based models utilize random horizontal flip [34] and multi-scale inputs (MS) [44, 55] as data augmentation methods, where multi-scale inputs randomly resizes the shorter side of the image to be between 480 and 800 pixels while keeping the longer side of the image not exceeding 1333 pixels. PVTv2, P2T, and ResNet-based models are trained with random horizontal flip and single-scale inputs (SS) [44], where single-scale inputs resizes the shorter side of the image to be 800 pixels while keeping the longer side of the image not exceeding 1333 pixels.

RetinaNet [41]and Cascade Mask R-CNN [2]. We test ResNet+MSCSA on RetinaNet and Cascade Mask R-CNN. On both detectors, we apply $1\times$ schedule, random horizontal flip, and single-scale inputs. Moreover, the models are trained using SGD as the optimizer with a mini-batch of 16 images, an initial learning rate of 0.02, a momentum of 0.9, a weight decay of 0.0001, and 500 linear warm-up iterations.

Deformable DETR [84]. We also test ResNet+MSCSA on Deformable DETR. Following its original setting, the models are trained for 50 epochs with random horizontal flip and multi-scale inputs while the learning rate decrease by $10\times$ after epoch 40, with AdamW [46] as the optimizer, a mini-batch of 32 images, an initial learning rate of 0.0002, and a weight decay of 0.0001.

C.3 ADK20k Segmentation

Implementation. All the models for ADK20k Segmentation are implemented based on MMSegmentation [11].

TopFormer [81]. Following the segmentation setting from TopFormer¹⁰, the proposed segmentation head in TopFormer is applied. The models are trained for 160k iterations using AdamW [46] as the optimizer with a mini-batch of 16 images, an input size of 512×512 , a weight decay of 0.01, a poly learning rate scheduler with a power of 1.0, and 1500 linear warm-up iterations. Moreover, the initial learning rate for TopFormer-T-based models is 0.0003, while the one for TopFormer-B-based modes is 0.00012. For data augmentation, random crop [34], random horizontal flip [34], and photometric distortions [34] are applied.

PVTv2 [65]. PVTv2-based models utilize Semantic FPN [33] for ADE20k segmentation. The models are trained for 40k iterations using AdamW [46] as the optimizer with a mini-batch of 32 images, an input size of 512×512 with the same data augmentation method as TopFormer-based models have, an initial learning rate of 0.0002, a weight decay of 0.0001, and a poly learning rate scheduler with a power of 0.9.

D Additional Implementaion Details

D.1 Multi-Stage Cross-Scale Attention (MSCSA) Blocks

Our MSCSA block follows the pre-norm [63] setting that the normalization layer is applied to the input of every sub-layer. Recent work has demonstrated that removing the classification (CLS)

¹⁰<https://github.com/hustvl/TopFormer>

token [15, 17, 59] from attention blocks does not affect the performance [20, 7, 64, 21]. Hence, during the design of the MSCSA block, the CLS token is not applied and the overall attention block uses the BCHW tensor format for efficient implementations. For instance, all the Layer Normalization [1] layers in MSCSA blocks are replaced by the Batch Normalization [31] layers. All the linear projections are implemented by the 1×1 convolutions.

D.2 Cross-Scale Attention (CSA)

The CSA block applies the basic conv-attention setting of LeViT [20], reducing the number of channels in the query, key, and value tensors in order to save computation. The query and key tensors are further reduced to half the channel dimension of the value tensor. An additional Hardswish activation [27] is also added to the attention output to encourage the nonlinear transformation in the attention module.

Parallel Convolution Path (PCP). The attention mechanism is good at modeling long-range relationships. However, it cannot distinguish between long-range and short-range relationships, where the structural information [32] and local relationships [47] play a significant role in vision tasks. Inspired by HRViT [21], we add a parallel convolution path between the value tensor in original resolution \mathbf{V}_0 and the output of self-attention $\text{Attention}(\mathbf{Q}, \mathbf{K}, \mathbf{V})$ to preserve local information and act as the positional encoding. To be precise, the PCP module consists of a Hardswish [27] activation and a 3×3 depthwise convolution with padding size 1 and stride 1:

$$\text{ConvPath}(\mathbf{V}_0) = \text{DWConv}(\text{Hardswish}(\mathbf{V}_0)). \quad (8)$$

The Hardswish and depthwise convolution in PCP enable nonlinear inductive bias injection and local feature aggregation reinforcement. The modified self-attention now becomes

$$\text{ModifiedAttn}(\mathbf{Q}, \mathbf{K}, \mathbf{V}) = \text{Attention}(\mathbf{Q}, \mathbf{K}, \mathbf{V}) + \text{ConvPath}(\mathbf{V}_0). \quad (9)$$